ATLAS CONF Note

ATLAS-CONF-2023-008

27th March 2023

Measurement of isolated photon plus multi-jet correlations in Pb+Pb and *pp* collisions at 5.02 TeV with ATLAS

The ATLAS Collaboration

This note presents a measurement of isolated photon plus multi-jet correlations in 1.72 nb^{-1} of Pb+Pb data and 260 pb^{-1} of *pp* data, both at 5.02 TeV, with the ATLAS detector. Events containing a photon with transverse momentum (p_{T}) in the range 90–180 GeV and at least two $R = 0.2$ jets with $p_{\text{T}} > 30$ GeV are selected for study. The medium-induced modification of the multi-jet system is explored with three new observables describing the kinematic relationship between a photon and a jet pair in the opposite azimuthal direction. The distributions are reported in *pp* collisions and in Pb+Pb collisions with different centrality intervals, along with their ratios between Pb+Pb and *pp* collisions. The results are compared to the predictions from a theoretical model of jet quenching.

ATLAS-CONF-2023-008
31 March 2023

1 Introduction

Collisions of ultra-relativistic heavy ions at the Large Hadron Collider (LHC) and the Relativistic Heavy Ion Collider (RHIC) produce a state of matter called the quark–gluon plasma (QGP) where quarks and gluons exist outside of the colorless configurations that define typical cold matter. Studies of this hot-and-dense state of deconfined partons have revealed a number of interesting characteristics: collective motion well described by relativistic hydrodynamic flow, sequential suppression of bound quarkonia states, and the suppression of observed final state products such as jets from hard-scattered partons [1]. This last phenomenon was first observed at RHIC with the study of large transverse momentum (p_{T})[1] hadrons [2] and subsequently at the LHC with fully reconstructed jets [3]. It is interpreted as the result of the color-opaque medium interacting with and attenuating the energy of these energetic quarks and gluons produced in the initial collision prior to the formation of the medium. For a recent full review of jet studies in the QGP at both colliders, see Ref. [4].

Measurements of jet quenching are a key part of understanding the structure and nature of the QGP. By comparing the kinematics of jets produced in Pb+Pb collisions to the well-measured characteristics of jets produced in *pp* collisions, the induced modifications from the QGP interacting with the developing parton shower can be studied. While many studies of modified jet production have been performed [5–10], there are unresolved questions on the exact nature of parton-medium interactions. These include questions on how much energy is lost to interactions with medium partons on a per color-charge basis, how the energy loss depends on parton flavor, and whether there is a minimum distance between color charges before the medium can resolve them as separate and independent [11, 12].

The measurements presented in this note address these questions by studying events containing an isolated photon with its transverse momentum balanced by at least two distinct jets, γ + 2 jets + X. As the photon has no color charge, it sets the scale of the initial hard scattering that produced it and the balancing multijet system, without any biases on this selection from the quenching of the photon kinematics. Such studies in Pb+Pb have been performed previously by ATLAS [13] and CMS [14] for photon-tagged inclusive jets, i.e. γ + 1 jet + X, where the production is dominated by a mixture of the leading order photon+jet matrix elements (direct) and from fragmentation photons. In these previous measurements, all jets are included in the yield, and thus the modification of per-photon-normalized distributions cannot be interpreted on a per-jet basis. However, in combination with an explicit study of the whole multijet configuration, this data should guide theoretical extraction of the per-color-charge energy loss induced by the medium. In addition, the multijet system typically produces one quark and one gluon jet opposite the photon, such that measurements of the jet–jet energy asymmetry could probe the parton color-charge dependence to medium interactions. Finally, studies as a function of the angle between the jet pair can be used to probe the existence of the color coherence regime.

This measurement considers three new observables defined by the photon and all jet pairs opposite the photon in azimuth. Within a given photon+jet pair, "1" or "leading" denotes the jet of higher p_{T}, and "2" or "subleading" denotes the jet of lower p_{T}. The photon is denoted by γ and its transverse momentum by $p_{\mathrm{T},\gamma}$. The new observables are the ratio of the magnitude of the two-jet vector p_{T} to that of the photon ($x_{\mathrm{JJ}\gamma}$), the

[1] ATLAS uses a right-handed coordinate system with its origin at the nominal interaction point (IP) in the centre of the detector and the z-axis along the beam pipe. The x-axis points from the IP to the centre of the LHC ring, and the y-axis points upwards. Cylindrical coordinates (r, ϕ) are used in the transverse plane, ϕ being the azimuthal angle around the z-axis. The pseudorapidity is defined in terms of the polar angle θ as $\eta = -\ln\tan(\theta/2)$. Angular distance is measured in units of $\Delta R \equiv \sqrt{(\Delta\eta)^2 + (\Delta\phi)^2}$.

difference between the two jet p_{T} values divided by that of the photon ($A_{\mathrm{JJ}\gamma}$), and the angle between the jet pair (ΔR_{JJ}), in events containing a photon and at least two jets. More explicitly, these are defined as:

$$x_{\mathrm{JJ}\gamma} = (\vec{p}_1 + \vec{p}_2)_{\mathrm{T}}/p_{\mathrm{T},\gamma}, \tag{1}$$

$$A_{\mathrm{JJ}\gamma} = (p_{\mathrm{T},1} - p_{\mathrm{T},2})/p_{\mathrm{T},\gamma}, \tag{2}$$

$$\Delta R_{\mathrm{JJ}} = \sqrt{\Delta\phi_{1,2}^2 + \Delta\eta_{1,2}^2}. \tag{3}$$

In events containing more than two candidate jets, the photon is considered with each possible jet pair separately, and thus a given jet can take on the leading or subleading role in the different $\gamma + 2$ jets $+X$ combinations. The distributions are normalized to the number of photons.

The measurements presented in this note are performed using *pp* reference data taken in 2017 corresponding to an integrated luminosity of 260 pb^{-1}, and Pb+Pb data taken in 2018 corresponding to an integrated luminosity of 1.72 nb^{-1}, both at 5.02 TeV. Events that contain an isolated photon with transverse momentum ($p_{\mathrm{T},\gamma}$) in the range $90 < p_{\mathrm{T},\gamma} < 180$ GeV and at least two $R = 0.2$ jets in the azimuthally opposite hemisphere ($\Delta\phi_{\mathrm{jet},\gamma} > \pi/2$) with $p_{\mathrm{T}} > 30$ GeV are studied. In addition to jets specifically associated with the initial hard process that produced the photon, the Pb+Pb events contain "combinatoric background" jets arising from uncorrelated hard-scatterings or UE fluctuations. A novel multijet mixed-event procedure, developed specifically for this analysis, is employed to correct for these contributions in the data. The results are reported as per-photon yields, differential in the three observables $x_{\mathrm{JJ}\gamma}$, $A_{\mathrm{JJ}\gamma}$, and ΔR_{JJ}, in *pp* and Pb+Pb collisions. The ratios of the Pb+Pb distributions to those in *pp* are used to characterize parton energy loss in the QGP and are compared to theoretical models.

2 ATLAS detector

The ATLAS experiment [15] at the LHC is a multipurpose particle detector with a forward–backward symmetric cylindrical geometry and a near 4π coverage in solid angle. It consists of an inner tracking detector surrounded by a thin superconducting solenoid providing a 2 T axial magnetic field, electromagnetic and hadron calorimeters, and a muon spectrometer. The inner tracking detector covers the pseudorapidity range $|\eta| < 2.5$. It consists of silicon pixel, silicon microstrip, and transition radiation tracking detectors. Lead/liquid-argon (LAr) sampling calorimeters provide electromagnetic (EM) energy measurements with high granularity. A steel/scintillator-tile hadron calorimeter covers the central pseudorapidity range ($|\eta| < 1.7$). The endcap and forward regions are instrumented with LAr calorimeters for both the EM and hadronic energy measurements up to $|\eta| = 4.9$. The muon spectrometer surrounds the calorimeters and is based on three large superconducting air-core toroidal magnets with eight coils each. The field integral of the toroids ranges between 2.0 and 6.0 T m across most of the detector. The muon spectrometer includes a system of precision tracking chambers and fast detectors for triggering. A zero-degree calorimeter (ZDC) was situated at $|\eta| > 8.3$ during Pb+Pb data-taking and is mostly sensitive to spectator neutrons from the fragmenting nuclei in Pb+Pb collisions.

A two-level trigger system is used to select events. The first-level trigger is implemented in hardware and uses a subset of the detector information to accept events at a rate below 100 kHz. This is followed by a software-based trigger that reduces the accepted event rate to 1 kHz on average depending on the data-taking conditions. An extensive software suite [16] is used in data simulation, in the reconstruction and analysis of real and simulated data, in detector operations, and in the trigger and data acquisition systems of the experiment.

3 Data selection, reconstruction, and simulation

The datasets, physics object reconstruction, and simulation samples used in this measurement are identical to those used in a previous measurement of photon-tagged jet production [17], and are briefly summarized here.

Events in data are selected for analysis using triggers requiring a reconstructed photon with p_{T} above 35 GeV (20 GeV) in pp (Pb+Pb) collisions [18, 19]. These triggers sample the full luminosity delivered in both 2017 pp and 2018 Pb+Pb collisions, and are fully efficient for the photon selection used in this analysis. Photons are reconstructed following the method used previously in Pb+Pb collisions [13, 20], which applies the procedure used in pp collisions [21] after an event-by-event estimation and subtraction of the underlying event (UE) contribution to the energy deposited in each calorimeter cell [22]. Photon candidates must pass shower shape requirements [23] designed to reject those arising from neutral meson decays and the start of hadronic showers in the electromagnetic calorimeter, and to be isolated by requiring an upper limit of 3 GeV on the sum of the transverse energy (after UE subtraction) in calorimeter cells within $\Delta R < 0.3$.

Jets are reconstructed following the procedure previously used in Pb+Pb collisions [5, 22]. The anti-k_t algorithm [24, 25] with distance parameter $R = 0.2$ is applied to cells in all calorimeter layers combined into $\Delta\eta \times \Delta\phi = 0.1 \times \pi/32$ logical towers. The contribution to the energy deposited in towers by the UE is estimated on an event-by-event basis, and the tower kinematics are iteratively updated to subtract the UE contribution, which is then re-estimated. The resulting jets are corrected using simulation to account for the response of the calorimeter to jets [26], and then using *in situ* studies of jets recoiling against photons, Z bosons, and jets in other regions of the calorimeter in pp collisions [13] for the absolute response in data.

The Pb+Pb event centrality is defined by the total sum of the transverse energy in the forward calorimeters, $\Sigma E_{\mathrm{T}}^{\mathrm{FCal}}$. Events in different ranges of $\Sigma E_{\mathrm{T}}^{\mathrm{FCal}}$ are associated with an underlying geometric configuration according to a Monte Carlo (MC) Glauber simulation [27] using the same event selection criteria as in previous ATLAS analysis [28]. This analysis uses three centrality intervals corresponding to the following fractions of the $\Sigma E_{\mathrm{T}}^{\mathrm{FCal}}$ distribution in minimum-bias events: 0–10% ("central" events, with a large nuclear overlap), 10–30%, and 30–80% ("peripheral" events).

MC simulations of photon+jet events are used to evaluate the performance of the photon and jet reconstruction and to correct the measured distributions for detector effects. For pp data, the main MC sample consists of Pythia8.2 [29] events. These include contributions from both direct and fragmentation photons and are produced with the A14 tune [30] and the NNPDF 2.3 LO parton distribution function (PDF) set [30]. These events are simulated [16] within ATLAS using GEANT4 [31] and are digitized and reconstructed in a manner identical to that in data. To simulate photon+jet events in Pb+Pb data, the above events are overlaid at the detector-hit level with a sample of Pb+Pb data events recorded with minimum-bias and high-activity triggers, and the combination is reconstructed as a single event. These "Pb+Pb data overlay" events are reweighted to match the observed $\Sigma E_{\mathrm{T}}^{\mathrm{FCal}}$ distribution for photon+jet events in Pb+Pb data.

The JEWEL (Jet Evolution With Energy Loss) 2.2.0 [32] MC generator, which models the jet quenching process in the QGP, is used to produce predictions to compare with the data. JEWEL is based on Pythia6 [33], but modifies the parton shower evolution via interactions with a dynamic QGP medium. Notably, when run in "vacuum mode", JEWEL reproduces the results of the Pythia6 generator for

pp collisions. JEWEL was run using the photon+jet hard scattering process [34], which includes only direct (leading order) photon production.

4 Analysis

The signal definition for the measurement presented here includes events with an isolated photon in the range $90 < p_{\mathrm{T},\gamma} < 180$ GeV and $|\eta^{\gamma}| < 2.37$ (excluding the barrel-to-endcap transition region of $1.37 < |\eta^{\gamma}| < 1.52$), and at least two $R = 0.2$ jets with $30 < p_{\mathrm{T}} < 501$ GeV and $|\eta^{\mathrm{jet}}| < 2.8$ that are in the azimuthal hemisphere opposite to the photon, $\Delta\phi_{\mathrm{jet},\gamma} = \left|\phi^{\mathrm{jet}} - \phi^{\gamma}\right| > \pi/2$. For each event passing this initial selection, the photon plus every possible combination of two jets is considered as a set. For each set of a candidate photon plus two jets, two further criteria are required: (1) the two jet axes must be separated by $\Delta R_{\mathrm{JJ}} > 0.4$, and (2) the four-vector sum of the two jets must have an azimuthal separation $\Delta\phi_{\mathrm{JJ}\gamma} > 7\pi/8$ from the photon. Since at tree level a direct photon plus two partons are expected to have approximately balancing momenta in the transverse plane, this last requirement reduces the rate of the combinatoric contributions while minimally impacting signal. After all such selections, initial distributions are formed for the three multijet observables $x_{\mathrm{JJ}\gamma}$, $A_{\mathrm{JJ}\gamma}$, and ΔR_{JJ} as defined in Eqs. 1-3.

In the candidate Pb+Pb events, a certain subset of the selected jets do not arise from the same hard scattering as the photon, but rather from an unrelated nucleon–nucleon scattering, or from jets which are reconstructed from localized fluctuations of the UE. These background jets are produced predominantly at low p_{T} and isotropically with respect to the photon. Such background jets can influence the observables by forming a jet plus background-jet pair, or even background-jet plus background-jet pair, and are included in the raw distributions. The influence of these jets on the observables is removed statistically using a mixed-event subtraction procedure. However, unlike the simpler procedures used for photon plus inclusive jet analyses [13, 17], a new technique is developed to account for the multi-jet observables in this measurement. This method is described below.

For each signal event (consisting of a photon plus at least two jets), two minimum-bias ("mixed") Pb+Pb data events are chosen which have similar centrality and the elliptic flow angle as the signal event, and thus have on average the same distribution of background jets. The distributions above are then constructed using three different combinations of the photon and jets in the signal event and the jets in the mixed event, as follows:

1. In the first step, the photon is considered together with all the jets in the first mixed event. This contribution fully accounts for the background-jet plus background-jet pairs which occur in data.

2. In the second step, for each signal jet, the photon plus that one signal jet and all the jets in the first mixed event are analyzed. This contribution accounts for the jet plus background-jet yield in data. However, since the jet from the signal event may itself be a background jet, this estimated background will generally include background-jet (from the signal event) plus background-jet (from the first mixed event) pairs. Since these background–background pairs are from different events, this contribution is not present in data. Therefore, an additional third step is needed to correct for the over-estimate of the background in this step.

3. In the third step, for each jet in the first mixed event, the photon plus that one mixed-event jet, and plus all the jets in the second mixed event, are considered. This contribution accounts for the

background-jet plus background-jet pairs from different events which is introduced by the second step.

For each observable, the per-photon yields from steps one and two are subtracted from the initial yields, and the yields from step three are added (to correct the background over-subtraction in step two), to produce a set of combinatoric-background-subtracted distributions. This procedure is first developed and tested using a toy MC approach in which the photons, signal jets, and background jets were represented by simple vectors. In this case, the background subtraction procedure results in a recovery of the true jet–jet yield within statistical uncertainties. The procedure is then tested using the PYTHIA plus Pb+Pb data overlay events (described in Sec. 3), where reconstructed jets matched to a PYTHIA generator-level jet are taken to be the signal jets, and the other jets in the event, i.e., those in the original Pb+Pb data event, were the background jets. In this case, complications such as the potential merging of jets at reconstruction level results in some residual non-closure of the background procedure, which is taken as a systematic uncertainty in the measurement (discussed in Sec. 5). The observed background correction in Pb+Pb data is of comparable magnitude to the signal in 0-10% events, and is greatest at large $A_{\mathrm{JJ}\gamma}$, large ΔR_{JJ}, and the tails of the $x_{\mathrm{JJ}\gamma}$ distribution. In these regions, the non-closure and corresponding systematic can be as large as 20%.

An additional background arises from photons from neutral meson and other decays. The purity of the selected photons is estimated following the data-driven, double-sideband method widely used in ATLAS photon measurements [35–38], and is 80–95% depending on the collision system and $p_{\mathrm{T},\gamma}$. The contribution to the jet–jet yields from this background is estimated in data and statistically subtracted using the same method as in previous measurements [13, 17, 20] and briefly summarized here. An inverted set of photon selection requirements designed to enhance the contribution from background is used to select events and the analysis is repeated, including the combinatoric background subtraction. The resulting jet–jet yields in these background events are scaled according to the estimated photon purity, and statistically subtracted from the yields made with the nominal photon selection.

Finally, an unfolding procedure is applied to data to correct for the kinematic bin migration introduced by detector resolution effects and for the finite reconstruction and selection efficiency. This correction is performed using the iterative Bayesian method [39] in the RooUnfold [40] software package. The simulation samples described in Sec. 3 are used to produce response matrices in pp and Pb+Pb collisions. Simulation is also used to test the unfolding procedure by using half of the simulation to construct response matrices while treating the other half as data to be unfolded and compared to truth kinematics. For each of the three observables, the unfolding is performed in three dimensions: the given observable (for example, $x_{\mathrm{JJ}\gamma}$), $p_{\mathrm{T},\gamma}$, and $p_{\mathrm{T},2}$. The latter two variables are included since the response along the observable axis is found to be particularly dependent on their values. The kinematic distributions are constructed in a wider range than the region in which the final results are reported, to allow for the unfolding to properly account for the migration into and out of the measurement region. Before the unfolding procedure is applied, the events in simulation are first reweighted to better describe the distributions as observed in data. The number of iterations is typically two or three depending on the observable and event class, and is chosen by minimizing the quadrature sum of the statistical uncertainties with the change in the distributions from the previous iteration.

5 Systematic Uncertainty

The sources of systematic uncertainty in this measurement are those associated with the photon, jet, background subtraction, and unfolding components. The uncertainties are typically evaluated by repeating the full analysis chain with a given systematic variation, which may result in, e.g., a different response matrix for the unfolding or a different reconstructed-level distribution.

The photon- and jet-related sources of uncertainties are the same as those used in a previous measurement of photon-tagged jet production in Pb+Pb and *pp* collisions [17], and are only summarized here. The photon-related uncertainties include those on the photon energy scale and resolution [41], their identification and isolation [23], and purity [13]. The jet-related uncertainties include the baseline uncertainties on the energy scale and resolution for $R = 0.4$ jets used for measurements in 13 TeV *pp* collisions [42–45], with additional sources [6, 46] accounting for the modified jet reconstruction procedure used in a heavy-ion environment, the smaller jet parameter $R = 0.2$, the data-taking conditions in 5.02 TeV running, the quark/gluon composition of photon+jet events at this collision energy, and the potential impact of jet quenching on the calorimeter response to jets.

The uncertainty associated with the mixed-event background subtraction procedure, present only for Pb+Pb collisions, is evaluated using input from the closure test of the procedure in the Pb+Pb data overlay simulation described in Sec. 4. For each of the three observables, the differences between the background-subtracted distribution and the reconstructed-level signal distribution in simulation are applied to the data bin-by-bin. The unfolding is then performed on these modified input distributions.

The uncertainty associated with the unfolding procedure has three components. The first is the sensitivity to the initial distributions used in the iterative unfolding, which is evaluated by using the simulation samples without reweighting to the data. Second, the reconstructed jet p_{T} threshold is raised from 30 GeV to 35 GeV, but still unfolded to the original kinematic range. Such a variation was used in Ref. [6] as a check against residual background jet contamination at low jet p_{T}. Finally, the impact of finite statistics in the simulation sample is evaluated with a toy re-sampling technique implemented in the RooUnfold package. This last component is much smaller than the statistical uncertainties in the data.

For the measurements in Pb+Pb data, the total uncertainties are similar for each observable and are typically 20–40%, but reaching as high as 100% in the low-yield tails. The photon isolation and purity, the combinatoric background subtraction, and the unfolding uncertainties have similar values and are co-dominant. For the *pp* measurement, the total uncertainties are typically 5–10%, with the jet energy scale and the unfolding uncertainties (which include an observed unfolding non-closure from simulation study) being dominant. Variations for sources common to the Pb+Pb and *pp* data are considered together when evaluating the ratio of distributions in these systems. This results in a modest reduction of the uncertainties in the Pb+Pb/*pp* ratio compared to the relative uncertainties just in the Pb+Pb per-photon yields.

Figure 1 shows the contributions of various sources to the systematic uncertainty on the ratio of Pb+Pb 0-10%/*pp* in each of the three observables. In general, the dominant uncertainties come from mixing non-closure, photon isolation and purity, and unfolding, with additional contributions coming from jet and photon energy scale/resolution. In the tails of the distributions the total relative systematic uncertainty can reach 100%.

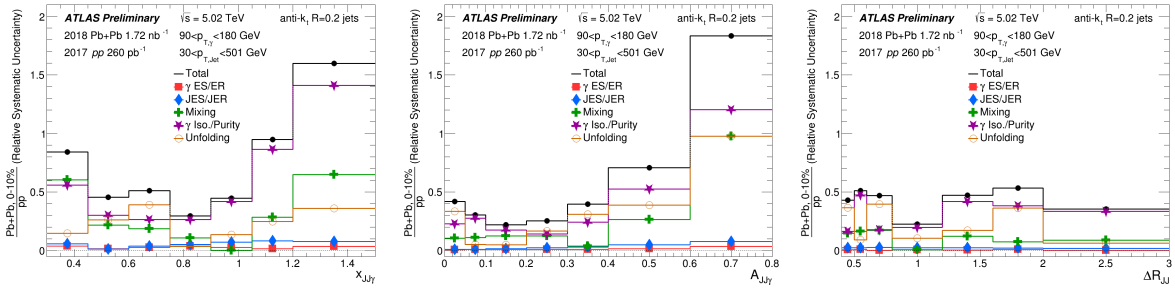

Figure 1: Relative systematic uncertainties on the ratio of the $x_{\mathrm{JJ}\gamma}$ (left), $A_{\mathrm{JJ}\gamma}$ (center), and ΔR_{JJ} (right) distribution between 0–10% Pb+Pb and *pp* events. Correlations in systematics betweeen the Pb+Pb and pp are accounted for in evaluating the ratio.

6 Results

Figure 2 shows the normalized yields as functions of the three observables ($x_{\mathrm{JJ}\gamma}$, $A_{\mathrm{JJ}\gamma}$, and ΔR_{JJ}) in *pp* collisions. The $x_{\mathrm{JJ}\gamma}$ distribution is observed to be strongly peaked near unity, representing the approximate vector momentum balance between the photon and the two jets. In previous measurements of photon plus inclusive jet production by ATLAS [13] and CMS [14], the distributions of $x_{\mathrm{J}\gamma}$=$p_{\mathrm{T,jet}}/p_{\mathrm{T},\gamma}$ had a significant per-photon yield at low values of $x_{\mathrm{J}\gamma}$ ($x_{\mathrm{J}\gamma} < 0.5$), corresponding to topologies where the photon was not well-balanced by only a single jet. This feature also complicated the interpretation of the analogous distribution in Pb+Pb data. By considering the vector sum of the two jets, the $x_{\mathrm{JJ}\gamma}$ observable presented here results in a distribution which is falling on both sides of the peak.

The prediction of the JEWEL MC model and Pythia8 are compared to the *pp* data distributions in Figure 2. The JEWEL model is effectively the same as Pythia6 when run in vacuum mode but includes only direct photons whereas Pythia8 includes direct and fragmentation photons, as mentioned earlier. Both JEWEL and Pythia8 are scaled by a factor of 1.2 to better match the per-photon overall yield between data and MC. In measurements of photon plus multi-jet production in *pp* collisions at 13 TeV [47], this factor was needed to bring the simulation into better agreement with the data, and is adopted for this measurement and comparison. Both the JEWEL and Pythia8 predictions qualitatively describe the shapes of the distributions, but with different levels of agreement depending on the generator, observable, and measured region. Since the Pythia generator is frequently used as the baseline for describing *pp* collisions in contemporary jet quenching calculations, these deviations from the measured *pp* data should be taken into account before interpreting the predicted modification of the distributions in Pb+Pb collisions due to jet quenching.

Figure 3 shows the measured $x_{\mathrm{JJ}\gamma}$ distribution in Pb+Pb collisions for different centrality intervals, with yields from *pp* collisions for comparison and Pb+Pb/*pp* ratio in the bottom panel. For the peripheral 30–80% Pb+Pb events, where QGP effects are expected to be the smallest, the $x_{\mathrm{JJ}\gamma}$ distribution is similar to that in *pp* events, albeit with a slightly reduced magnitude and the peak position shifted to lower $x_{\mathrm{JJ}\gamma}$ values. Going from the peripheral to the more central 10–30% and 0–10% events, the total integral of the distribution continues to decrease and the position of the peak continues to shift leftward, though notably the latter observation is weaker given the large systematic uncertainties in central Pb+Pb. In all centrality selections, the Pb+Pb per-photon yield compared to that in *pp* collisions is consistent with an increasing suppression at increasingly larger values of $x_{\mathrm{JJ}\gamma}$. In the most central Pb+Pb events, the rate of events in

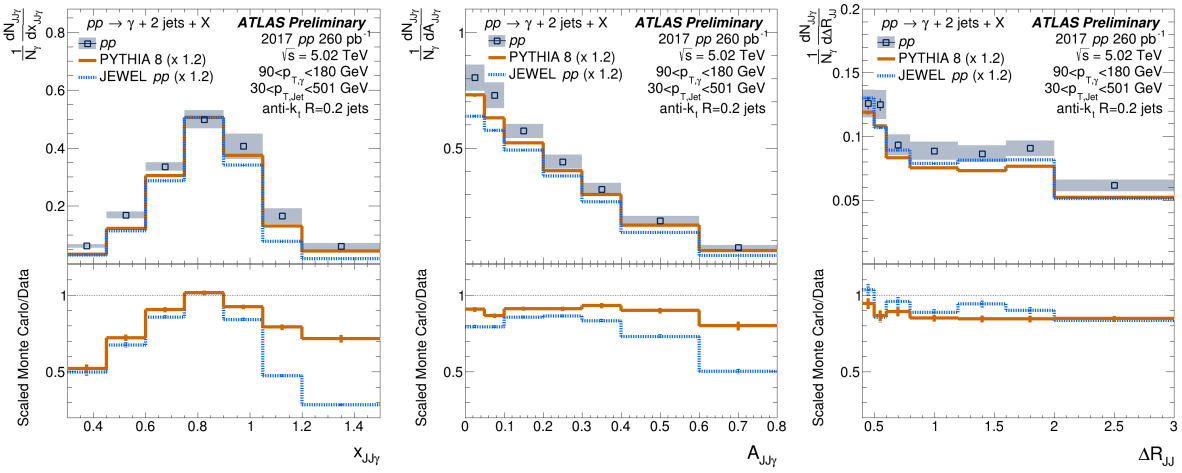

Figure 2: Measured distributions of $x_{\mathrm{JJ}\gamma}$ (left), $A_{\mathrm{JJ}\gamma}$ (center), and ΔR_{JJ} (right) in photon plus multi-jet events in *pp* collisions at 5.02 TeV (markers). Statistical and systematic uncertainties are plotted as vertical lines and shaded boxes around each point, respectively. The data are compared to the distributions in the JEWEL (blue dashed lines) and PYTHIA8 (red solid lines) generators, which are scaled by the factor shown in the legend. The ratios of the generator distributions to those in data are shown in the bottom panels.

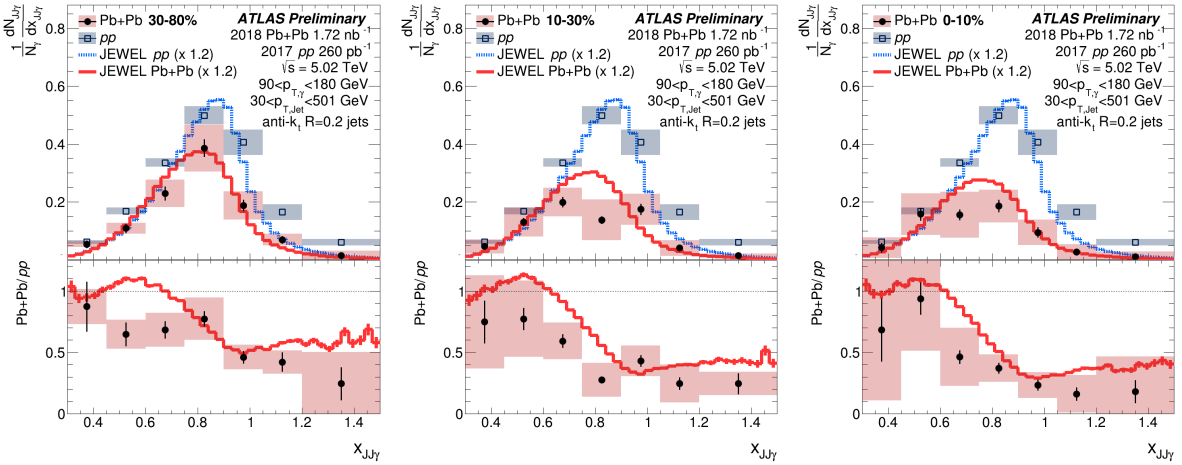

Figure 3: Measured distributions of $x_{\mathrm{JJ}\gamma}$ in photon plus multi-jet events in Pb+Pb events at 5.02 TeV. The different panels show different Pb+Pb centrality selections (open squares), with the distribution in *pp* collisions (solid circles, same every panel). Statistical and systematic uncertainties are plotted as vertical lines and shaded boxes around each point, respectively. Also shown are the predictions of the JEWEL model for *pp* events (blue line) and Pb+Pb events (red line), which have been scaled by a factor of 1.2. The ratios of the Pb+Pb to *pp* distributions are shown in the bottom panels.

which the two jets have a total momentum comparable to or larger than that of the photon, i.e., the region $x_{\mathrm{JJ}\gamma} > 0.75$, is suppressed by more than a factor of two compared to that in *pp* collisions.

The smaller per-photon yield in Pb+Pb collisions may be understood as a manifestation of jet quenching through two mechanisms. First, both jets may generally lose energy, thus decreasing the resulting $x_{\mathrm{JJ}\gamma}$ value compared to what it would have been in a *pp* collision with the same hard-scattering kinematics.

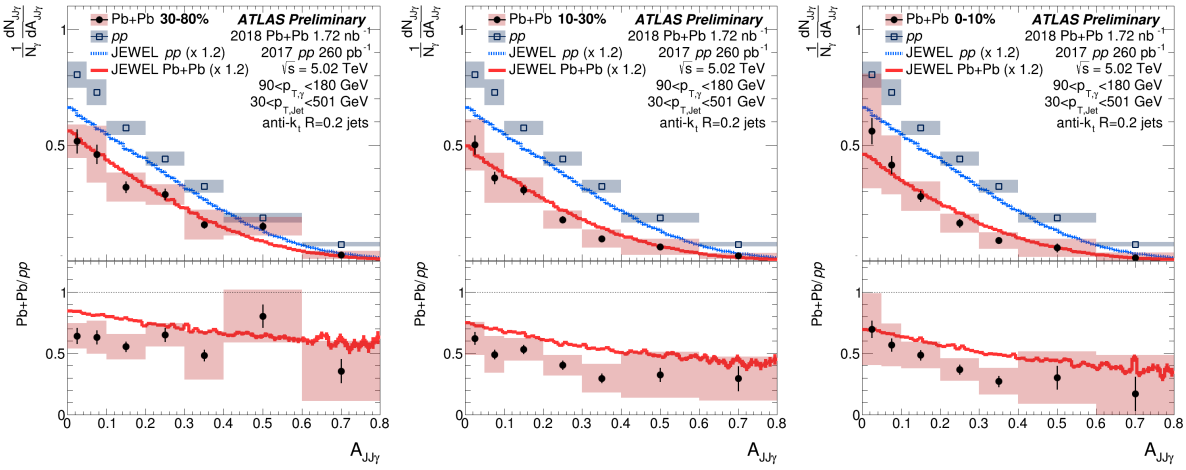

Figure 4: Measured distributions of $A_{\mathrm{JJ}\gamma}$ in photon plus multi-jet events in Pb+Pb events at 5.02 TeV. The different panels show different Pb+Pb centrality selections (open squares), with the distribution in *pp* collisions (solid circles, same every panel). Statistical and systematic uncertainties are plotted as vertical lines and shaded boxes around each point, respectively. Also shown are the predictions of the JEWEL model for *pp* events (blue line) and Pb+Pb events (red line), which have been scaled by a factor of 1.2. The ratios of the Pb+Pb to *pp* distributions are shown in the bottom panels.

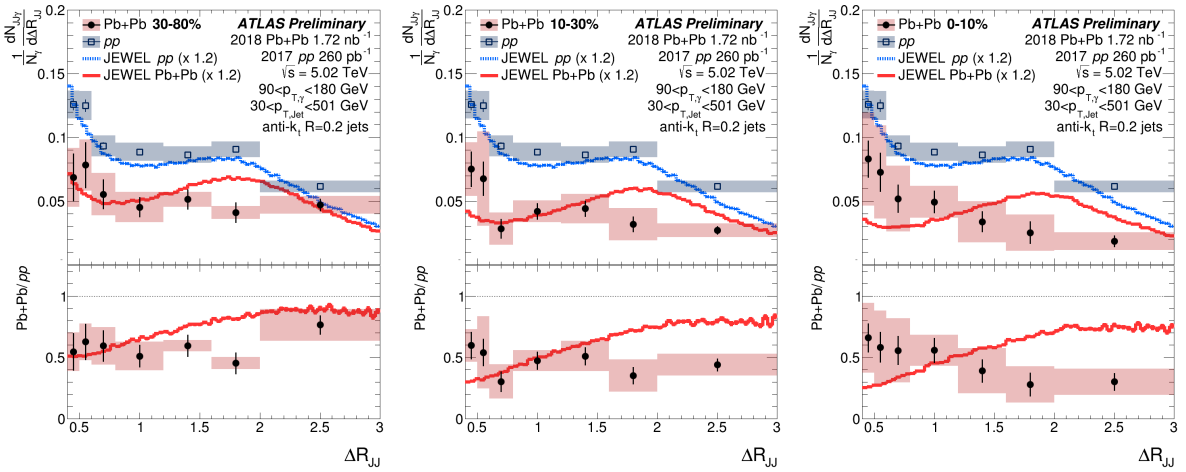

Figure 5: Measured distributions of ΔR_{JJ} in photon plus multi-jet events in Pb+Pb events at 5.02 TeV. The different panels show different Pb+Pb centrality selections (open squares), with the distribution in *pp* collisions (solid circles, same every panel). Statistical and systematic uncertainties are plotted as vertical lines and shaded boxes around each point, respectively. Also shown are the predictions of the JEWEL model for *pp* events (blue line) and Pb+Pb events (red line), which have been scaled by a factor of 1.2. The ratios of the Pb+Pb to *pp* distributions are shown in the bottom panels.

Additionally, if at least one jet loses enough energy that it falls below the 30 GeV kinematic selection, the Pb+Pb event is not selected for analysis and thus does not contribute to the distribution.

Figures 4 and 5 show the measured $A_{\mathrm{JJ}\gamma}$ and ΔR_{JJ} distributions, respectively, for the Pb+Pb and *pp* data, with the ratio between Pb+Pb and *pp* shown in the bottom panels. For both observables, the Pb+Pb

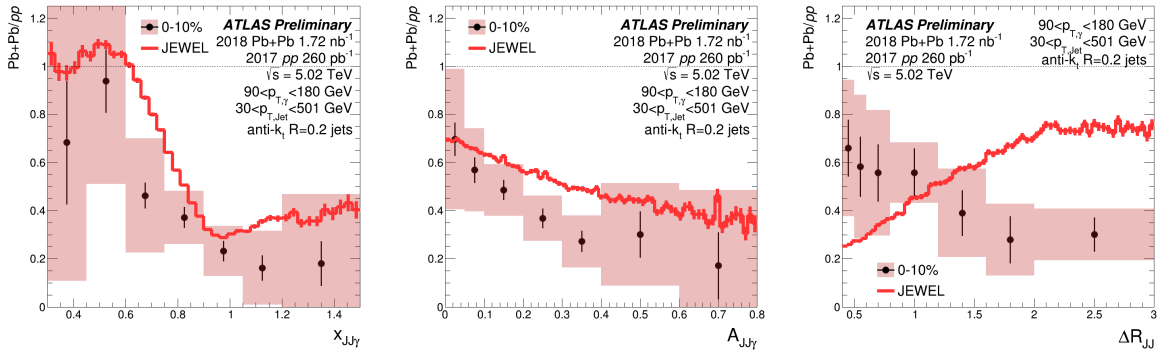

Figure 6: Measured ratio of the $x_{\mathrm{JJ}\gamma}$ (left), $A_{\mathrm{JJ}\gamma}$ (center), and ΔR_{JJ} (right) distribution between 0–10% Pb+Pb and *pp* events, compared to the predictions of JEWEL 2.2.0 (dashed line). Statistical and systematic uncertainties on the data are plotted as vertical lines and shaded boxes around each point, respectively. The data and and predictions shown here are identical to those in the bottom-right panels of Figs. 3–5.

distributions are suppressed with respect to those in *pp* collisions to a degree that increases with centrality. In the most central 0–10% events, the suppression relative to *pp* collisions is consistent with becoming stronger at larger values of $A_{\mathrm{JJ}\gamma}$ or ΔR_{JJ}, corresponding to cases where the two jets have very different p_{T} values or have a large angular separation, respectively. The suppression of asymmetric configurations in Pb+Pb compared to *pp* is related to the observed leftward shift of the peak $x_{\mathrm{JJ}\gamma}$ value in 0-10% Pb+Pb. An $x_{\mathrm{JJ}\gamma}$ value of 0.5 for the given $p_{\mathrm{T},\gamma}$ selection means the composite jet pair most likely has 45 GeV, leaving very little room for asymmetry before falling below jet p_{T} cut thresholds. This illustrates the complex interdependence of the three observables.

The predictions of JEWEL are compared to the measured distributions for the three observables in *pp* and Pb+Pb data in Figures 3–5. They are scaled by a factor of 1.2 to better match the *pp* data, but this scaling cancels in the Pb+Pb/*pp* ratios. Figure 6 shows the comparison of the measured ratios for 0–10% Pb+Pb and *pp* collisions with the predictions of JEWEL as functions of the three observables. The JEWEL predictions provide a qualitatively good description of the Pb+Pb/*pp* ratios for the $x_{\mathrm{JJ}\gamma}$ and $A_{\mathrm{JJ}\gamma}$ distributions, but underestimate the overall magnitude of the suppression for these two observables. However, JEWEL has the opposite trend as a function of ΔR_{JJ}, where instead configurations with jet pairs separated by a smaller angle are more suppressed than those with a larger one. This last comparison illustrates how these new observables may be used to provide novel tests of jet quenching models.

7 Conclusion

This note presents a measurement of photon plus multi-jet correlations in *pp* and Pb+Pb data at 5.02 TeV, collected in 2017 and 2018, respectively, with the ATLAS detector at the LHC. Three observables describing the kinematic relationship between the photon and a pair of jets are defined, with the motivation to test different aspects of the parton-medium interactions in the quark–gluon plasma. Distributions as functions of these observables are reported in *pp* events and in Pb+Pb events in different centrality intervals. In Pb+Pb events, the per-photon multi-jet yield is strongly suppressed compared to that in *pp* events in a way that depends on the centrality interval and observable. The predictions of the JEWEL jet quenching model are compared to the measurements; the predictions show a qualitatively good description of the data,

but underestimate the overall magnitude of the suppression and fail to describe its dependence on the angle between the two jets. Together with further theoretical comparisons, measurements as functions of these novel observables may shed new light on the microscopic process of energy loss in the QGP.

References

[1] W. Busza, K. Rajagopal and W. van der Schee,
Heavy Ion Collisions: The Big Picture, and the Big Questions,
Ann. Rev. Nucl. Part. Sci. **68** (2018) 339, arXiv: 1802.04801 [hep-ph] (cit. on p. 2).

[2] PHENIX Collaboration, *Suppression of Hadrons with Large Transverse Momentum in Central Au + Au Collisions at* $\sqrt{s_{\mathrm{NN}}}$ = 130GeV, Phys. Rev. Lett. **88** (2 2001) 022301,
URL: https://link.aps.org/doi/10.1103/PhysRevLett.88.022301 (cit. on p. 2).

[3] ATLAS Collaboration, *Measurements of the Nuclear Modification Factor for Jets in Pb+Pb Collisions at* $\sqrt{s_{NN}}$ = 2.76 *TeV with the ATLAS Detector*, Phys. Rev. Lett. **114** (2015) 072302, arXiv: 1411.2357 [hep-ex] (cit. on p. 2).

[4] L. Cunqueiro and A. M. Sickles, *Studying the QGP with Jets at the LHC and RHIC*,
Prog. Part. Nucl. Phys. **124** (2022) 103940, arXiv: 2110.14490 [nucl-ex] (cit. on p. 2).

[5] ATLAS Collaboration, *Measurement of the nuclear modification factor for inclusive jets in Pb+Pb collisions at* $\sqrt{s_{NN}}$ = 5.02 *TeV with the ATLAS detector*, Phys. Lett. B **790** (2019) 108,
arXiv: 1805.05635 [hep-ex] (cit. on pp. 2, 4).

[6] ATLAS Collaboration,
Measurements of the suppression and correlations of dijets in Pb+Pb collisions at $\sqrt{s_{NN}}$ = 5.02 *TeV*,
(2022), arXiv: 2205.00682 [nucl-ex] (cit. on pp. 2, 7).

[7] ATLAS Collaboration, *Measurements of azimuthal anisotropies of jet production in Pb+Pb collisions at* $\sqrt{s_{NN}}$ = 5.02 *TeV with the ATLAS detector*, Phys. Rev. C **105** (2021) 064903,
arXiv: 2111.06606 [nucl-ex] (cit. on p. 2).

[8] CMS Collaboration, *Measurement of transverse momentum relative to dijet systems in PbPb and pp collisions at* $\sqrt{s_{NN}}$ = 2.76 *TeV*, JHEP **01** (2016) 006, arXiv: 1509.09029 [hep-ex] (cit. on p. 2).

[9] CMS Collaboration,
Measurement of the Splitting Function in pp and PbPb collisions at $\sqrt{s_{NN}}$ = 5.02 *TeV*,
Phys. Rev. Lett. **120** (2018) 142302, arXiv: 1708.09429 [hep-ex] (cit. on p. 2).

[10] CMS Collaboration,
First measurement of large area jet transverse momentum spectra in heavy-ion collisions,
JHEP **05** (2021) 284, arXiv: 2102.13080 [hep-ex] (cit. on p. 2).

[11] J. Casalderrey-Solana, Y. Mehtar-Tani, C. A. Salgado and K. Tywoniuk,
New picture of jet quenching dictated by color coherence, Phys. Lett. B **725** (2013) 357,
arXiv: 1210.7765 [hep-ph] (cit. on p. 2).

[12] J. Casalderrey-Solana, G. Milhano, D. Pablos and K. Rajagopal, *Modification of Jet Substructure in Heavy Ion Collisions as a Probe of the Resolution Length of Quark-Gluon Plasma*,
JHEP **01** (2020) 044, arXiv: 1907.11248 [hep-ph] (cit. on p. 2).

[13] ATLAS Collaboration, *Measurement of photon-jet transverse momentum correlations in* 5.02 *TeV Pb+Pb and pp collisions with ATLAS*, Phys. Lett. B **789** (2019) 167,
arXiv: 1809.07280 [hep-ex] (cit. on pp. 2, 4–8).

[14] CMS Collaboration, *Study of jet quenching with isolated-photon+jet correlations in PbPb and pp collisions at* $\sqrt{s_{NN}} = 5.02$ *TeV*, Phys. Lett. B **785** (2018) 14, arXiv: 1711.09738 [hep-ex] (cit. on pp. 2, 8).

[15] ATLAS Collaboration, *The ATLAS Experiment at the CERN Large Hadron Collider*, JINST **3** (2008) S08003 (cit. on p. 3).

[16] ATLAS Collaboration, *The ATLAS Collaboration Software and Firmware*, ATL-SOFT-PUB-2021-001, 2021, URL: https://cds.cern.ch/record/2767187 (cit. on pp. 3, 4).

[17] ATLAS Collaboration, *Comparison of inclusive and photon-tagged jet suppression in 5.02 TeV Pb+Pb collisions with ATLAS*, (2022), arXiv: 2303.10090 [nucl-ex] (cit. on pp. 4–7).

[18] ATLAS Collaboration, *Performance of the ATLAS trigger system in 2015*, Eur. Phys. J. C **77** (2017) 317, arXiv: 1611.09661 [hep-ex] (cit. on p. 4).

[19] ATLAS Collaboration, *Performance of electron and photon triggers in ATLAS during LHC Run 2*, Eur. Phys. J. C **80** (2020) 47, arXiv: 1909.00761 [hep-ex] (cit. on p. 4).

[20] ATLAS Collaboration, *Comparison of Fragmentation Functions for Jets Dominated by Light Quarks and Gluons from pp and Pb+Pb Collisions in ATLAS*, Phys. Rev. Lett. **123** (2019) 042001, arXiv: 1902.10007 [hep-ex] (cit. on pp. 4, 6).

[21] ATLAS Collaboration, *Electron and photon performance measurements with the ATLAS detector using the 2015–2017 LHC proton–proton collision data*, JINST **14** (2019) P12006, arXiv: 1908.00005 [hep-ex] (cit. on p. 4).

[22] ATLAS Collaboration, *Measurement of the jet radius and transverse momentum dependence of inclusive jet suppression in lead–lead collisions at* $\sqrt{s_{NN}} = 2.76$ *TeV with the ATLAS detector*, Phys. Lett. B **719** (2013) 220, arXiv: 1208.1967 [hep-ex] (cit. on p. 4).

[23] ATLAS Collaboration, *Measurement of the photon identification efficiencies with the ATLAS detector using LHC Run 2 data collected in 2015 and 2016*, Eur. Phys. J. C **79** (2019) 205, arXiv: 1810.05087 [hep-ex] (cit. on pp. 4, 7).

[24] M. Cacciari, G. P. Salam and G. Soyez, *The anti-*k_t *jet clustering algorithm*, JHEP **04** (2008) 063, arXiv: 0802.1189 [hep-ph] (cit. on p. 4).

[25] M. Cacciari, G. P. Salam and G. Soyez, *FastJet user manual*, Eur. Phys. J. C **72** (2012) 1896, arXiv: 1111.6097 [hep-ph] (cit. on p. 4).

[26] ATLAS Collaboration, *Jet energy measurement and its systematic uncertainty in proton–proton collisions at* $\sqrt{s} = 7$ *TeV with the ATLAS detector*, Eur. Phys. J. C **75** (2015) 17, arXiv: 1406.0076 [hep-ex] (cit. on p. 4).

[27] M. L. Miller, K. Reygers, S. J. Sanders and P. Steinberg, *Glauber modeling in high energy nuclear collisions*, Ann. Rev. Nucl. Part. Sci. **57** (2007) 205, arXiv: nucl-ex/0701025 (cit. on p. 4).

[28] ATLAS Collaboration, *Prompt and non-prompt* J/ψ *and* $\psi(2S)$ *suppression at high transverse momentum in* 5.02 *TeV Pb+Pb collisions with the ATLAS experiment*, Eur. Phys. J. C **78** (2018) 762, arXiv: 1805.04077 [hep-ex] (cit. on p. 4).

[29] T. Sjöstrand, S. Mrenna and P. Skands, *A brief introduction to PYTHIA 8.1*, Comput. Phys. Commun. **178** (2008) 852, arXiv: 0710.3820 [hep-ph] (cit. on p. 4).

[30] ATLAS Collaboration, *ATLAS Pythia 8 tunes to 7 TeV data*, ATL-PHYS-PUB-2014-021, 2014, URL: https://cds.cern.ch/record/1966419 (cit. on p. 4).

[31] S. Agostinelli et al., *GEANT4–a simulation toolkit*, Nucl. Instrum. Meth. A **506** (2003) 250 (cit. on p. 4).

[32] K. C. Zapp, *JEWEL 2.0.0: directions for use*, Eur. Phys. J. C **74** (2014) 2762, arXiv: 1311.0048 [hep-ph] (cit. on p. 4).

[33] T. Sjöstrand, S. Mrenna and P. Z. Skands, *PYTHIA 6.4 physics and manual*, JHEP **05** (2006) 026, arXiv: hep-ph/0603175 (cit. on p. 4).

[34] R. Kunnawalkam Elayavalli and K. C. Zapp, *Simulating V+jet processes in heavy ion collisions with JEWEL*, Eur. Phys. J. C **76** (2016) 695, arXiv: 1608.03099 [hep-ph] (cit. on p. 5).

[35] ATLAS Collaboration, *Measurement of the inclusive isolated prompt photon cross section in pp collisions at $\sqrt{s} = 8$ TeV with the ATLAS detector*, JHEP **08** (2016) 005, arXiv: 1605.03495 [hep-ex] (cit. on p. 6).

[36] ATLAS Collaboration, *Measurement of the cross section for inclusive isolated-photon production in pp collisions at $\sqrt{s} = 13$ TeV using the ATLAS detector*, Phys. Lett. B **770** (2017) 473, arXiv: 1701.06882 [hep-ex] (cit. on p. 6).

[37] ATLAS Collaboration, *Measurement of the inclusive isolated prompt photons cross section in pp collisions at $\sqrt{s} = 7$ TeV with the ATLAS detector using 4.6 fb^{-1}*, Phys. Rev. D **89** (2014) 052004, arXiv: 1311.1440 [hep-ex] (cit. on p. 6).

[38] ATLAS Collaboration, *High-E_T isolated-photon plus jets production in pp collisions at $\sqrt{s} = 8$ TeV with the ATLAS detector*, Nucl. Phys. B **918** (2017) 257, arXiv: 1611.06586 [hep-ex] (cit. on p. 6).

[39] G. D'Agostini, *A multidimensional unfolding method based on Bayes' theorem*, Nucl. Instrum. Meth. A **362** (1995) 487, ISSN: 0168-9002 (cit. on p. 6).

[40] T. Adye, 'Unfolding algorithms and tests using RooUnfold', *Proceedings, 2011 Workshop on Statistical Issues Related to Discovery Claims in Search Experiments and Unfolding (PHYSTAT 2011)* (CERN, Geneva, Switzerland, 17th–20th Jan. 2011) 313, arXiv: 1105.1160 [physics.data-an] (cit. on p. 6).

[41] ATLAS Collaboration, *Electron and photon energy calibration with the ATLAS detector using 2015–2016 LHC proton–proton collision data*, JINST **14** (2019) P03017, arXiv: 1812.03848 [hep-ex] (cit. on p. 7).

[42] ATLAS Collaboration, *Jet energy measurement with the ATLAS detector in proton–proton collisions at $\sqrt{s} = 7$ TeV*, Eur. Phys. J. C **73** (2013) 2304, arXiv: 1112.6426 [hep-ex] (cit. on p. 7).

[43] ATLAS Collaboration, *Jet energy scale measurements and their systematic uncertainties in proton–proton collisions at $\sqrt{s} = 13$ TeV with the ATLAS detector*, Phys. Rev. D **96** (2017) 072002, arXiv: 1703.09665 [hep-ex] (cit. on p. 7).

[44] ATLAS Collaboration, *Jet energy resolution in proton–proton collisions at $\sqrt{s} = 7$ TeV recorded in 2010 with the ATLAS detector*, Eur. Phys. J. C **73** (2013) 2306, arXiv: 1210.6210 [hep-ex] (cit. on p. 7).

[45] ATLAS Collaboration, *Determination of jet calibration and energy resolution in proton–proton collisions at $\sqrt{s} = 8$ TeV using the ATLAS detector*, Eur. Phys. J. C **80** (2020) 1104, arXiv: 1910.04482 [hep-ex] (cit. on p. 7).

[46] ATLAS Collaboration,
Jet energy scale and its uncertainty for jets reconstructed using the ATLAS heavy ion jet algorithm, ATLAS-CONF-2015-016, 2015, URL: https://cds.cern.ch/record/2008677 (cit. on p. 7).

[47] ATLAS Collaboration, *Measurement of isolated-photon plus two-jet production in pp collisions at $\sqrt{s} = 13$ TeV with the ATLAS detector*, JHEP **03** (2020) 179, arXiv: 1912.09866 [hep-ex] (cit. on p. 8).